Journal of Pharmacy and Pharmacology, 2026, **78**, rgag044
https://doi.org/10.1093/jpp/rgag044
Advance access publication 6 May 2026
Research Paper

JPP Journal of Pharmacy and Pharmacology
OXFORD

Viscoelastic properties of polymer mixtures containing micro-ribbons and microfibres for the 3D printing of pharmaceutical dosage forms by fused deposition modelling

Marwan Algellay[1], Satyajit D. Sarker[2], Matthew Roberts[1], Lucy A. Bosworth[3], Touraj Ehtezazi[1,*]

[1]School of Pharmacy and Biomolecular Sciences, Liverpool John Moores University, Byrom Street, Liverpool L3 3AF, Merseyside, United Kingdom
[2]Centre for Natural Products Discovery (CNPD), School of Pharmacy and Biomolecular Sciences, Liverpool John Moores University, Byrom Street, Liverpool L3 3AF, Merseyside, United Kingdom
[3]Faculty of Health & Life Sciences, University of Liverpool, William Henry Duncan Building|6 West Derby Street, Liverpool L7 8TX, Merseyside, United Kingdom
*Corresponding author. School of Pharmacy and Biomolecular Sciences, Liverpool John Moores University, Byrom Street, Liverpool L3 3AF, United Kingdom. Email: t.ehtezazi@ljmu.ac.uk

Abstract

Objectives: **To match the disintegration time of conventional oral films with 3D printed fast-dissolving oral films (FDFs), micro-composites have been used in the formulation. However, in certain cases the 3D-printer failed to produce desired films.**

Methods: **The viscoelastic properties were evaluated for polyvinyl alcohol and polyvinylpyrrolidone filaments containing chitosan micro-ribbons and cellulose microfibres as micro-composites with the hypothesis that intermittent nozzle blockage was the mechanism responsible for the observed printing failures.**

Key findings: **Domination of loss modulus over storage modulus was observed for successful printing. Micro-composites improved the viscoelastic properties of filaments including filaments that failed to print. The novelty of this research was that poor viscoelastic properties could not be accounted for the failure of FDF 3D printing for formulations with high micro-composite contents. Filaments of these formulations exhibited rough surfaces with visible aggregates. These observations suggested intermittent nozzle blockage by aggregated micro-composites could have been the cause of 3D printing failure. This hypothesis was supported by successful printing when printer nozzle diameter increased.**

Conclusions: **The domination of loss modulus over storage modulus was essential for filaments to achieve successful FDF 3D printing. However, micro-composites at high concentrations in the formulation may induced nozzle blockage leading to printing failures.**

Keywords 3D printing, fused deposition modelling, viscoelastic properties, fast dissolving oral films, storage modulus, loss modulus, complex viscosity, micro-composites

Introduction

Amongst the most widely used 3D printing technologies, Fused Deposition Modelling (FDM) stands out for its application in drug product development. This method benefits from its affordability of FDM printing systems, making it an accessible option for researchers and manufacturers. Additionally, this technique enhances the ability to produce uniform drug products with precise control over their release rates by adjusting print parameters. The integration of hot-melt extrusion technology further broadens the potential applications of FDM in drug delivery development [1]. Whilst material extrusion-based additive manufacturing offers a wide range of applications, one common challenge lies in selecting the right polymers and printing parameters. The issue arises when certain composite materials lack essential viscoelastic, mechanical, and plastic properties necessary for successful printing, making it difficult to achieve desired results [2].

Rheology is the discipline concerned with the deformation and flow behaviour of materials, and viscosity represents a fundamental parameter describing the resistance of a material to flow [3]. The solid material must meet two critical mechanical requirements: Sufficient strength to avoid buckling and adequate surface hardness to resist damage from the extruder's feeding mechanism [4]. Knowledge of the optimal viscosity range for extrusion may facilitate predicting the printability of a new formulation. A useful method for testing the printability of a new melt formulation is to

Received: 18 December 2025. **Revised:** 24 March 2026. **Accepted:** 07 April 2026

compare its viscosity with that of a previously successful system using a rheometer. Notably, differing viscosity profiles do not necessarily preclude extrusion of the new molten formulation, as long as it exhibits similar viscosity at the operating shear rate [5].

The viscosity of a polymer melt is intricately influenced by the presence of additives, as well as the temperature and shear rate applied during melt extrusion. Therefore, it is crucial to investigate how temperature and angular frequency affect the flow behaviour and deformation of the molten mass. Whilst oscillatory rheology provides valuable insights into these dynamics, it has a limitation when simulating the shear rate and pressure generated by the rotating screw/filament feeding mechanism during melt extrusion, as the shear rate produced by an oscillatory rheometer is often significantly lower than in real-world processing conditions. Nevertheless, it is possible to conduct a preliminary evaluation of the effect of shear rate on viscosity by measuring complex viscosity as a function of angular frequency at a predetermined temperature and oscillation strain [6].

The storage modulus (G′) quantifies the energy stored and subsequently recovered, characterizing the elastic component of a material's response to shear deformation [7]. The loss modulus (G″) represents the energy dissipated in the form of heat, thereby describing the viscous aspect of a material's shear response. Crossover points, where G′ equals G″, correspond to shifts in the viscoelastic regime of the polymer melt [8].

Experimental findings from 3D printing via melt extrusion have revealed instances of instability, attributed to viscoelastic phenomena and wall slip effects inherent in the flow behaviour of polymer melts. This complexity has ultimately resulted in the failure of extrusion at elevated feeding rates and reduced printing temperatures [9]. The incorporation of multiwall carbon nanotubes (MWCNTs) into polylactic acid (PLA) at a concentration of 9 wt% resulted in a significant increase in viscosity, with values four times higher than those of neat PLA. This enhancement is attributed to the possible alignment of untangled, anisotropic MWCNTs along the flow direction, rendering the highly filled material resistant to flow. In contrast, the viscosity of graphene nanoplatelets (GNPs)/PLA nanocomposites in the shear thinning range exhibited values lower than those of neat PLA, particularly at high filler contents. This phenomenon is associated with a lubrication flow. The superior dispersion and stronger interfacial interactions between oxidized MWCNTs and PLA are believed contributing to this effect [10]. Notably, similar findings have been reported by Knauert *et al.* [11], who predicted that rod-like nanoparticles could produce the largest enhancements in shear viscosity. This may be attributed to the presence of polymer chains forming a bridge between the nanotubes, facilitated by interfacial polymer-filler interactions.

We previously reported the effects of adding micro-ribbons and cellulose microfibres in the 3D printing of fast-dissolving oral films (FDFs) by FDM [12]. We observed that certain formulations failed to successfully produce films by this 3D printing method, despite acceptable mechanical strength. Therefore, the research question was to determine whether unsuitable rheological properties or printer nozzle blockage caused unsuccessful printing. We hypothesized that nozzle blockage by micro-composites might have caused failure of 3D printing. Therefore, we conducted rheological tests as additional analytical framework to gain a deeper understanding of the flow behaviour and viscoelastic properties of filaments with micro-composite materials during 3D printing with FDM. This involved analyzing the loss, storage, and complex viscosity of both printable and non-printable formulations. We identified that, in addition to certain mechanical strengths required for filaments, nozzle blockage by micro-composite materials played a key role in successful 3D printing of the films. It should be noted that the extrusion process is a highly complex process in FDM 3DP and understanding viscoelastic measurements of molten feedstock are essential for predicting printability [3]. This approach does not directly evaluate the pressure-driven flow conditions within the printhead, nor does it capture the extensional flow components that arise in the converging nozzle geometry.

Materials and methods

Materials

Paracetamol, polyvinyl alcohol (PVA, Mw 89 000–98 000 D, 99% hydrolyzed), chitosan (low molecular weight), polyvinylpyrrolidone (PVP, Mw 40 000 and 10 000 D) polyethelene-oxide (PEO, Mw 100 000 and 200 000 D) and sodium triphosphate pentabasic (TPP) were purchased from Sigma-Aldrich (Dorset, UK). Croscarmellose sodium was acquired from Merck-chemicals (Darmstadt, Germany). Cellulose microfibres (Celova®) with three different surface areas (C500, C1000, and C2000 mm^2/g) were gifted from Healthy Suppliers Weidmann fibre technology (Rapperswil, Switzerland).

Methods

Preparation of filaments by hot-melt extrusion

Table 1 presents formulation compositions investigated in this work. Powders of excipients and active ingredient (paracetamol) were introduced into the Turbula-mixer (Type 2B; WAB, Muttenz, Switzerland) and blended at a speed of 42 rpm for 15 min to obtain a homogenized mixture [13]. The powder mixture was fed into a single-screw hot melt extruder (Noztek pro®) equipped with a counter-rotating screw with a speed of 30 rpm and a custom-made rod-shaped aluminium die (ø = 1.70 mm), to produce filaments. The diameter of filaments depended on the formulation, and they were in the range of 1.728 ± 0.085 mm to 1.948 ± 0.08 mm, and only those filaments were selected that had diameters less than 1.8 mm. The extrusion temperature was set at 170–180°C for PVA formulations and 120–130°C for PVP formulations [12]. The mechanical properties of the filaments were evaluated in our previous work [12].

3D printing of oral films

The films were primarily manufactured using a FDM Prusa® i3 MK3S 3D printer (Prague, Czech Republic). In addition, an RS PRO® IdeaWerk 3D Printer (RS Components Ltd, Northants, UK) was used for certain formulations (PVP formulations) due to a different gearing mechanism in this 3D printer. The film designs were created in stereolithographic format (.stl) by assisting of SolidWorks® 3DCAD software (Dassault Systèmes SolidWorks Corp., Waltham, MA). Square plain films measured 20 mm × 20 mm and width a thickness of 0.2 mm. The.stl design files were exported to the PrusaSlicer® software (version 2.3.3; Prague, Czech Republic) to use with the Prusa® i3 MK3S printer. The printing parameters were 100% infill for plain films and 50%

Table 1 The composition of formulations (W/W%).

Formulations	PVP 40 K	PEO 100 K	PVA	PCM	Croscar mellose	Chi-MR	C 500	C 1000	C2000
F1	0	0	100	0	0	0	0	0	0
F2	0	0	70	30	0	0	0	0	0
F3	0	0	63	30	7	0	0	0	0
F4	0	0	62	30	7	1	0	0	0
F5	0	0	61	30	7	2	0	0	0
F6	0	0	60	30	7	3	0	0	0
F7	0	0	69	30	0	1	0	0	0
F8	0	0	68	30	0	2	0	0	0
F9	0	0	67	30	0	3	0	0	0
F10	40	30	0	30	0	0	0	0	0
F11	33	30	0	30	7	0	0	0	0
F12	33	29.8	0	30	7	0.2	0	0	0
F13	33	29.5	0	30	7	0.5	0	0	0
F14	33	29	0	30	7	1	0	0	0
F15	33	28	0	30	7	2	0	0	0
F16	33	27	0	30	7	3	0	0	0
F17	33	25	0	30	7	5	0	0	0
F18	33	25	0	30	7	0	5	0	0
F19	33	25	0	30	7	0	0	5	0
F20	33	25	0	30	7	0	0	0	5
F21	33	20	0	30	7	0	10	0	0

triangular infill for mesh films, two shells, 0.10 mm layer height, and an extruder temperature of 200°C. The non-extrusion travel move speed was 60 mm/s, with an infill travel speed of 30 mm/s and a printer bed temperature of 50°C.

Printing time was 3 min for a plain film and 2 min for a mesh film. In addition, MakerWave® software processed the same plain film.stl files, as well as a mesh shape to be used with the RS Pro® 3D printer (RS Components Ltd, United Kingdom). The RS Pro® printer parameters were: 100% infill, two shells, and extruder temperature of 180–200°C. A slow printing speed was used, as the printer had only three printing speeds: fast, standard, and slow. The print bed temperature was set at 30°C for the RS® 3D Pro printer and 45°C for the Prusa 3D printer. Printing times for mesh and plain films was 90 and 120 s, respectively, on the RS 3D printer. The printer heads contained 0.4 mm and 1 mm diameter extruder nozzles. The mechanical properties of the films were determined in our previous work [12].

Rheological measurements

The viscoelastic behaviour of filaments was evaluated using an HR-10 oscillatory rheometer (TA instruments, USA) equipped with a Peltier plate and a 25 mm parallel plate geometry, with a gap height fixed at 0.4 mm (Fig. S1). Also, the gap was adjusted to 1 mm in order to examine high-concentration cellulose microfibre filaments. The amplitude of oscillatory shear was determined to ensure tests were conducted in the linear viscoelastic range, which was defined by an oscillatory amplitude sweep test at a constant angular frequency (ω) of 6.28 rad/s and strain (γ) range from 1% to 100% [14]. The filament geometry consisted of cylindrical samples with a length of 0.5 cm and a diameter of 1.75 mm. In this work low oscillatory strain was applied to ensure measurements were within linear viscoelastic regions. The temperatures were selected according to the printing process. The PVA formulations were tested at 200°C, whilst the PVP formulations were tested at 190°C. All samples were tested in triplicate, and loss moduli, storage moduli, and complex viscosity were measured.

Scanning electron microscopy

FEI inspect® scanning electron microscope (SEM) was used to study the surface morphology of Chi-MRs, cellulose microfibres, and 3D printed films at 20 kV accelerating voltage. The dry samples were mounted on aluminium stubs and gold coated using an Emitech K550 (Ashford, UK) sputter coater.

Statistical analysis

The SPSS [IBM SPSS Statistics Version 30.0.0.0 (172)] was used to conduct non-parametric comparisons using the *Kruskal-Wallis test* on viscoelastic parameters (loss modulus, storage modulus, and complex viscosity) at 100% strain, to simulate flow of molten polymer at the nozzle. The significance level was adjusted by applying the Bonferroni correction.

Results

Figure 1 presents loss and storage moduli, and complex viscosity for the F1 formulation (pure PVA). A distinct separation between storage modulus and loss modulus was observed, with the loss modulus being the dominant property. This figure suggests ideal viscoelastic properties for printing a film using FDM (Prusa 3D printer). The relevant photos are provided in the Supplementary

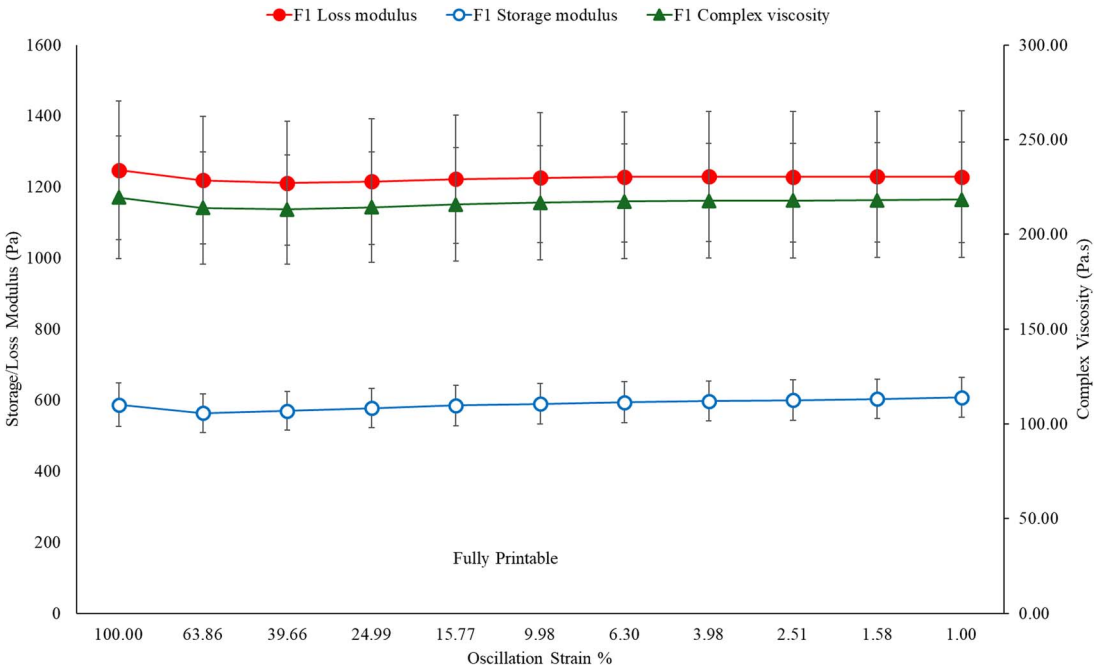

Figure 1 The viscoelastic properties of formulation F1 which contained only PVA. Data are presented as mean ± SD (n = 3).

Data, as well as viscoelastic parameters at 100% strain as bar charts for clearer comparisons.

Figure 2a compares the storage and loss moduli for formulations F2-F9. The addition of active ingredient (paracetamol) and other excipients (croscarmellose and Ch-R) considerably reduced both loss and storage moduli compared to the formulation F1, and the statistical difference (adjusted $P = .034$) was only observed between storage moduli of formulation F1 and F4. The addition of 7% croscarmellose (F3) slightly reduced both loss and storage moduli compared to formulation F2 (adjusted $P = 1.000$, for both storage and loss moduli). The addition of chitosan (Ch-MR) at 1% w/w further reduced only loss modulus compared to Formulation F3. All the films of formulations F2 to F4 were fully printed (Fig. S2). In contrast, increasing Ch-MR to 2% w/w (formulation F5) increased the loss modulus compared to formulation F4, although the difference did not reach the statistical level (adjusted $P = 1.000$) with minimal change to storage modulus. Despite a considerable gap between storage and loss moduli, formulation F5 was partially printed (Fig. S2). Increasing Ch-MR to 3% w/w for formulation F6 further increased the loss modulus, but also the storage modulus compared to formulation F5 (adjusted $P = 1.000$). Notably, the error bars considerably increased compared to previous formulations, suggesting inconsistent rheological regions within the filament. Formulation F6 was also partially printed (Fig. S2), despite a considerable gap between storage and loss moduli. Examining the filament surfaces of formulations F5 and F6 (Fig. S2) demonstrated aggregated patches, suggesting that Ch-MR did not disperse uniformly within the formulation, leading to potential nozzle blockage during printing. Removing croscarmellose from formulations F4–F6 (i.e. formulations F7–F9) only added formulation F8 to the list of successfully printable formulations. Formulation F8 exhibited a decrease in both loss and storage moduli (Fig. 2b) by increasing the strain, suggesting re-arrangements of aggregates at high strains, which could explain the successful printing of formulation F8. Filament of formulation F8 showed a smoother surface compared to formulation F5 (Fig. S2). These data suggest that croscarmellose contributed to inconsistent rheological regions within the filaments.

Formulations F10-F12 (PVA replaced with PVP and PEO) were printed successfully as expected from the above trend, which had significant gaps between storage and loss moduli (Fig. 3 for formulation F10, and Fig. 4a for formulations F11 and F12). Interestingly, formulation F12 contained 0.2% Ch-MR, and both storage and loss moduli unexpectedly reduced compared to formulations F5 and F11 (Figs 4a and S6) with statistically significant differences with formulation F10 at 100% strain (adjusted $P = .34$ for loss modulus and adjusted $P = .028$ for storage modulus). Increasing Ch-MR concentrations in formulations F13-F17 increased both storage and loss moduli compared to formulation F12, creating a desirable gap between them for successful printing; however, formulations F13 and F14 were only partially printed (Fig. S3), and formulations F15–F17 failed to print entirely. These observations suggest nozzle blockage at higher Ch-MR concentrations could have played a key role in unsuccessful printing. The addition of cellulose microfibres in formulations F18–F20 up to 5% w/w resulted in producing filaments with a smooth surface and printing films with fewer defects, and formulation F20 produced the best films (Fig. S3). These formulations also exhibited desired viscoelastic properties (Fig. 4b). However, increasing the cellulose microfibre C500 concentration to 10% w/w (formulation F21) failed to print full films with a 0.4 mm nozzle (Fig. S4), despite demonstrating desirable viscoelastic behaviour (Figs 4b and S7). On the other hand, formulation F21 films were printed successfully by changing the nozzle diameter to 1 mm (Fig. S3), suggesting possible nozzle blockage with a 0.4 mm nozzle diameter. Increasing the Peltier plate gap distance to 1 mm significantly (adjusted $P < .05$) reduced both storage and loss moduli compared to Peltier plate gap distance at 0.4 mm at 100% strain for formulation F21 (Fig. S7).

The complex viscosities of formulations F2–F21 versus strain are illustrated in Fig. 5 and at 100% strain in Figs S8–S10. Only

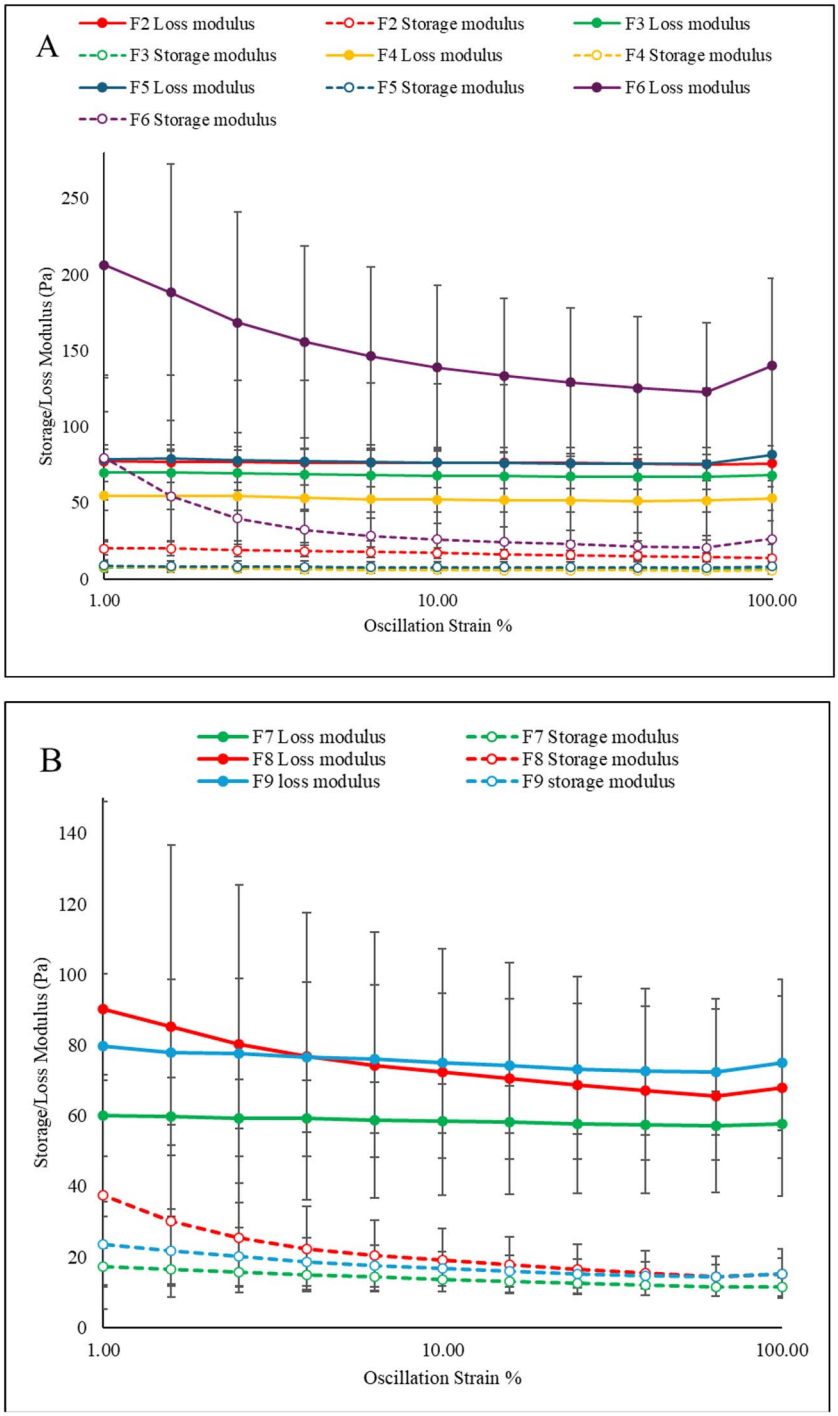

Figure 2 The loss and storage moduli versus strain of formulations: (a) F2–F6, (b) F7–F9. Data are presented as mean ± SD (n = 3).

formulations F6 (Fig. 5a) and F21 (Fig. 5b, 0.4 mm Peltier plate gap) demonstrated shear thinning viscosity by increasing strain. The complex viscosities of Formulations F10 and F12 reached statistically significant differences at 100% strain (adjusted $P = .034$). Formulation F21 at 0.4 mm Peltier plate gap also reached a statistically significant (adjusted $P = .01$) higher viscosity compared to the same formulation at 1 mm Peltier plate gap at 100% strain (Fig. S10). These observations suggest that the complex viscosity did not play a key role in the printability of these formulations.

Figure 6a compares the phase angles of formulation F1 to F9 versus strain. Formulation F1 showed a phase angle about 65°, whilst adding excipients and the active ingredient further increased the phase angle and reached a statistically significant different level between formulations F1 and F3 at 100% strain (adjusted $P = .013$). Figure 6a also shows that phase angles of formulation F6 fell between those of formulation F1 and F3, both of which were successfully printable, whilst formulation F6 was only partially printed. This observation highlights that the rheological properties were not the main reason for printing failure, but that other mechanisms were involved such as nozzle blockage by Ch-MR. Figure 6b illustrates phase-angle plots for formulations F10 to F21. The addition of cellulose microfibres

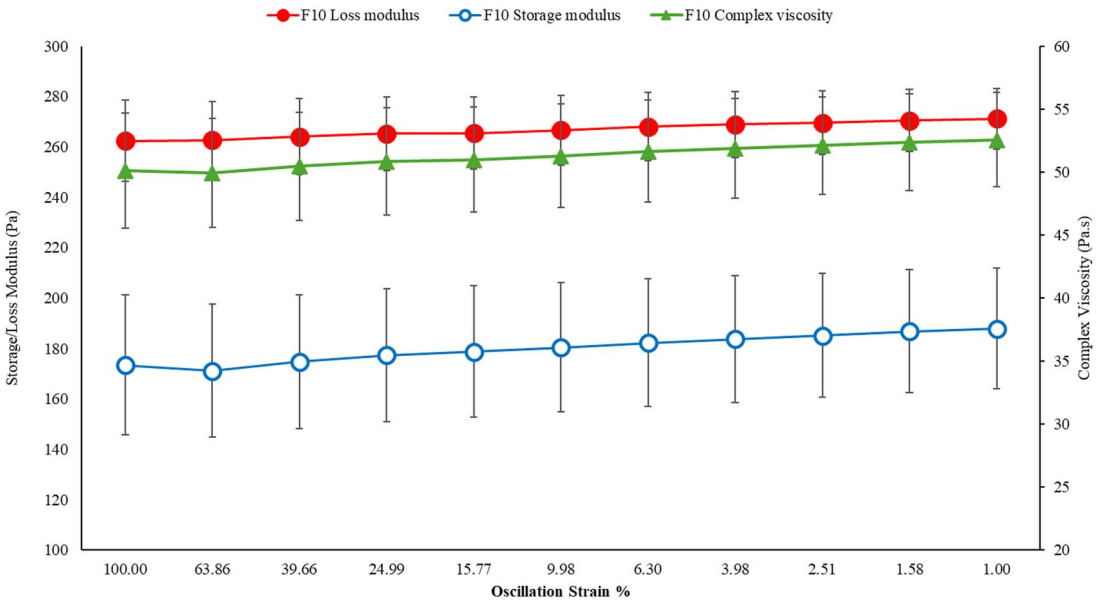

Figure 3 The viscoelastic properties of formulation F10, which contained PVP/PEO/PCM. Data are presented as mean ± SD (n = 3).

produced filaments with increased elasticity (indicated by decreasing phase angles), with the minimum phase angles observed for formulation F21 at a 1 mm Peltier plate gap. A similar trend was also observed for Ch-MRs (Fig. 6a).

Figure 7 demonstrates SEM images of Ch-MR (Fig. 7a) and C500 (Fig. 7b). Ch-MRs had diameters in the range of 7–50 μm, whilst C500 showed diameters in the range of 20–30 μm. The wide diameters of Ch-MRs and cellulose microfibres could block 400 μm printer nozzle at high concentrations, in particular if these microcomposites form aggregates in the molten polymer. It should be noted that a lack of feedability in the filaments (i.e. resistance to being fed through the printer head under higher mechanical pressure) was observed for formulations with high microcomposite concentrations, suggesting nozzle blockage rather than an increase in the viscosity of the molten polymer.

Discussion

The pure PVA sample (formulation F1) showed ideal viscoelastic behaviour, characterized by a dominant loss modulus and a clear distinction between storage and loss moduli, serving as a benchmark for successful printing performance, as also stated previously [15].

Comparing the outcomes of this work with the measured mechanical properties of the filaments in our previous study [12] shows that the mechanical strengths of filaments F11 and F16 were similar, whilst the rheological properties showed higher storage and loss moduli for formulation F16 compared to F11. Furthermore, formulation F7 (1% w/w Ch-MR) was printed successfully, whereas formulation F14 (also 1% w/w Ch-MR but in a different polymer matrix) failed to do so, despite both systems exhibiting desirable rheological profiles. This disparity arose from the superior mechanical integrity of formulation F7 compared to formulation F14 [12], indicating that rheological properties cannot fully capture the mechanical strength of filaments. Yuan *et al*. [16] reported that incorporating cellulose fibres can enhance the mechanical properties and processability of FDM filaments; an approach to enhance the structural characterizes of printed objects [17]. However, our results indicated the potential limitation of nozzle blockage by fibres.

In this work, a low angular velocity (6.28 rad/s) was applied to ensure that measurements were conducted within the linear viscoelasticity region, whilst high angular velocities have been considered for the flow of the molten polymer in the printer head [3]. The dominance of loss modulus over storage modulus was also observed at low angular velocities in FDM 3DP for successful printing [15], similar to our work.

Our results are in good agreement with the work of Ilieva *et al.*, who found that incorporating paracetamol and disintegrant additives into the polymer matrix resulted in a significant decrease in the PVA filament's overall viscosity and resistance to flow, relative to the control sample lacking the additives [18].

Increasing the amount of Ch-MR from 1% w/w to 3% w/w (formulations F4–F6, and F7–F9) gradually increased both loss and storage moduli; however, it introduced substantial variability at higher concentrations, evidenced by large error bars, demonstrating the formation of heterogeneous rheological regions within the filament. Whilst Rigotti *et al*. reported successful printing as the concentration of carbon nanotubes increased to 3% w/w [19]. Our results indicated nozzle blockage at higher concentrations of micro-ribbons and microfibres may lead to printing failure, which was also observed with increased fibre volume fraction in 3D printing [20]. This finding was supported by our microscopic analysis, which demonstrated wide Ch-MRs (7–50 μm) and cellulose micro-fibres (20–30 μm), which could block printer nozzle at high concentrations. Furthermore, increasing printer nozzle diameter led to successful printing of FDFs. In addition, photographs obtained from filaments (Supplementary Data) showed an uneven surface. Furthermore, the larger width of Ch-MR fibres (7–50 μm) physically obstructed the nozzle at higher Ch-MR concentrations, regardless of their favourable viscoelastic signatures. On the other hand, cellulose microfibres (C500) with narrower widths (20–30 μm) exhibited more favourable performance compared

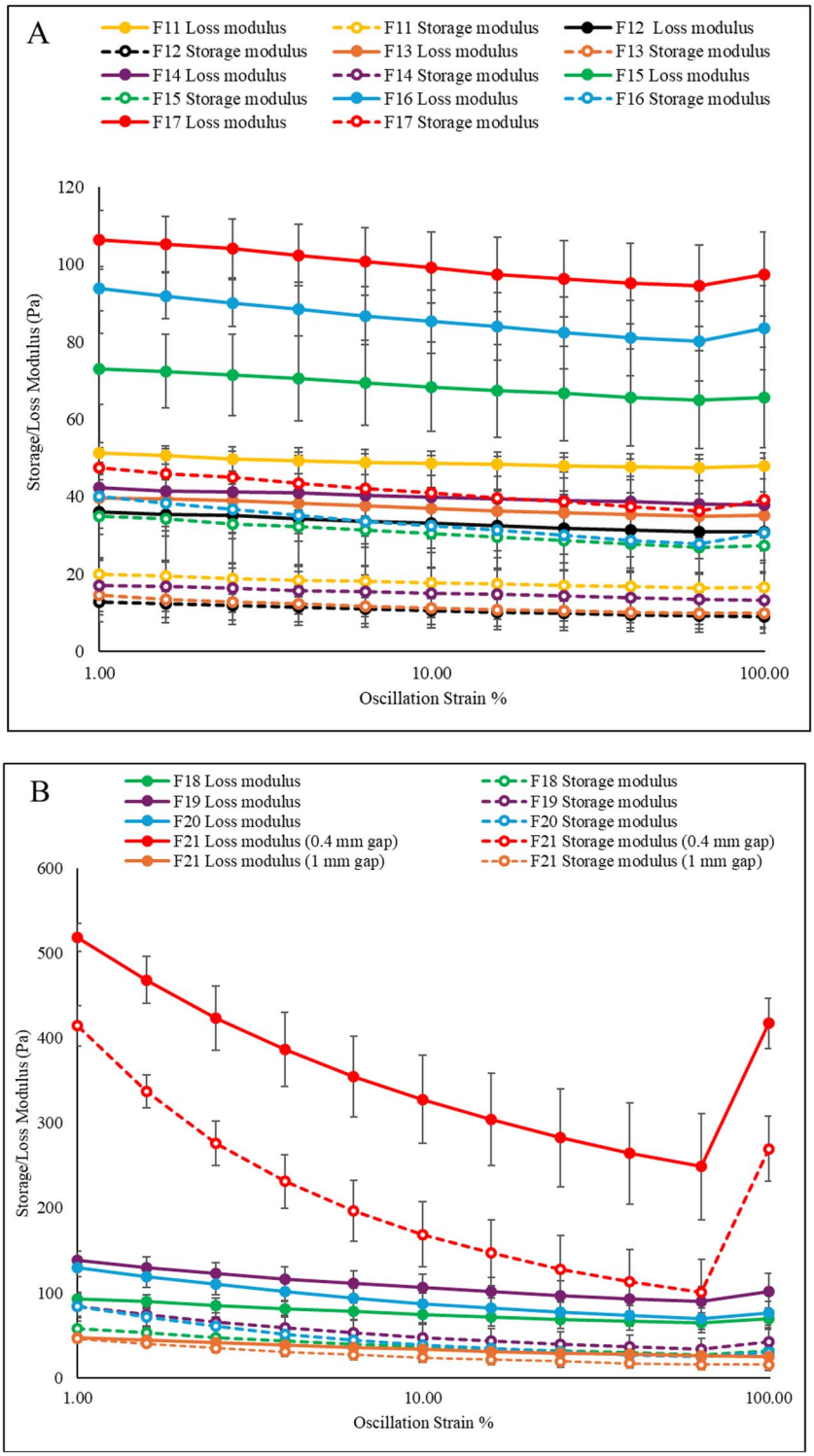

Figure 4 The loss and storage moduli versus strain of formulations: (a) F11–F17, (b) F18–F21. The loss and storage moduli of formulation F21 are given with 0.4 mm and 1 mm Peltier gaps. Data are presented as mean ± SD (n = 3).

to Ch-MR (∼50 μm) at higher concentrations. Zhang *et al.* also suggested that fibre length is expected to be the primary contributor to nozzle clogging [20]. Thus, nozzle diameter and micro-composite size play significant roles in shaping the characteristics of printed materials. Although a typical 0.4 mm nozzle diameter in FDM 3DP [21] can lead to enhanced resolution and mechanical properties [22], it also increases the likelihood of clogging when composite filaments are used. Therefore, when micro-composites are added to the formulation of filaments, SEM images or close-up observations of the filament may indicate whether nozzle blockage could prevent successful printing.

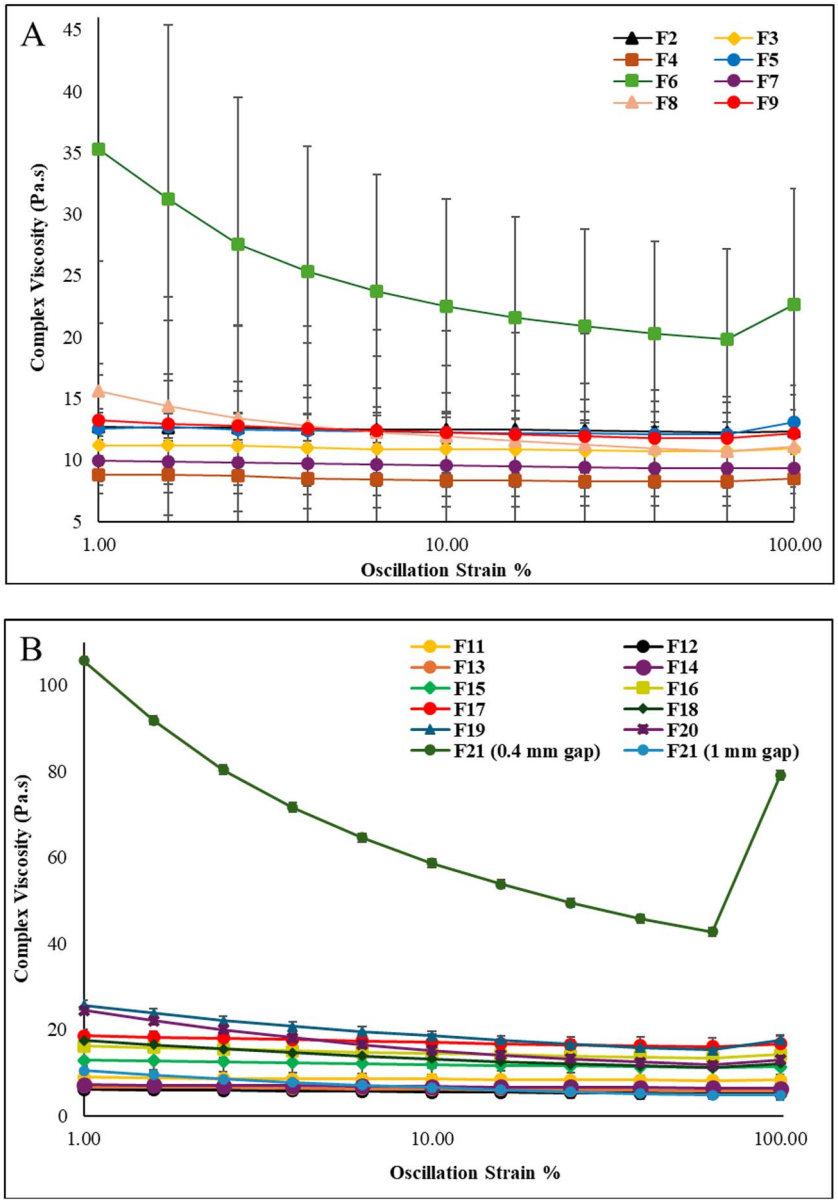

Figure 5 The complex viscosity versus strain of formulations: (a) F2–F9, (b) F11–F21. The complex viscosities of formulation F21 are given with 0.4 mm and 1 mm Peltier gaps. Data are presented as mean ± SD (n = 3).

Our results did show shear thinning viscosity at low angular frequencies when strain increased, but only for formulations containing high percentages of Ch-MR (2 and 3% w/w) or high concentrations of cellulose microfibre (10% w/w and 0.4 mm Peltier plate gap), whereas not pure PVA, suggesting the formation and breakdown of Ch-MR network at high strain values. Shear thinning viscosity has been reported for molten PLA polymer at 200°C [9].

In this study we conducted amplitude sweep test to identify viscoelastic transition of molten polymer formulations from solid-like to liquid-like behaviour, i.e. the crossover point at which storage modulus falls below the loss modulus [23]. This was to identify if structural breakdowns occurred within the polymer in the printhead initiating polymer flow. The results demonstrated that the poor printability observed in certain polymer formulations could not be attributed to an absence of viscoelastic transition from solid-like to liquid like-behaviour.

This study has several limitations that warrant acknowledgement. Nozzle blockage should be confirmed through direct visualization of the nozzle using imaging techniques such as X-ray analysis [24]. Furthermore, a more comprehensive characterization of viscoelastic properties would be beneficial, such as the application of frequency sweep test to assess structural stability of molten polymers. In addition, improvements should be made regarding better dispersion of micro-ribbons and microfibres in the formulations. The produced filaments should be evaluated for feedability such as the effects of feeding force on feeding rate [9].

Conclusions

This study reveals that the printability of PVA-based filaments in FDM is intricately linked to the interplay between viscoelastic

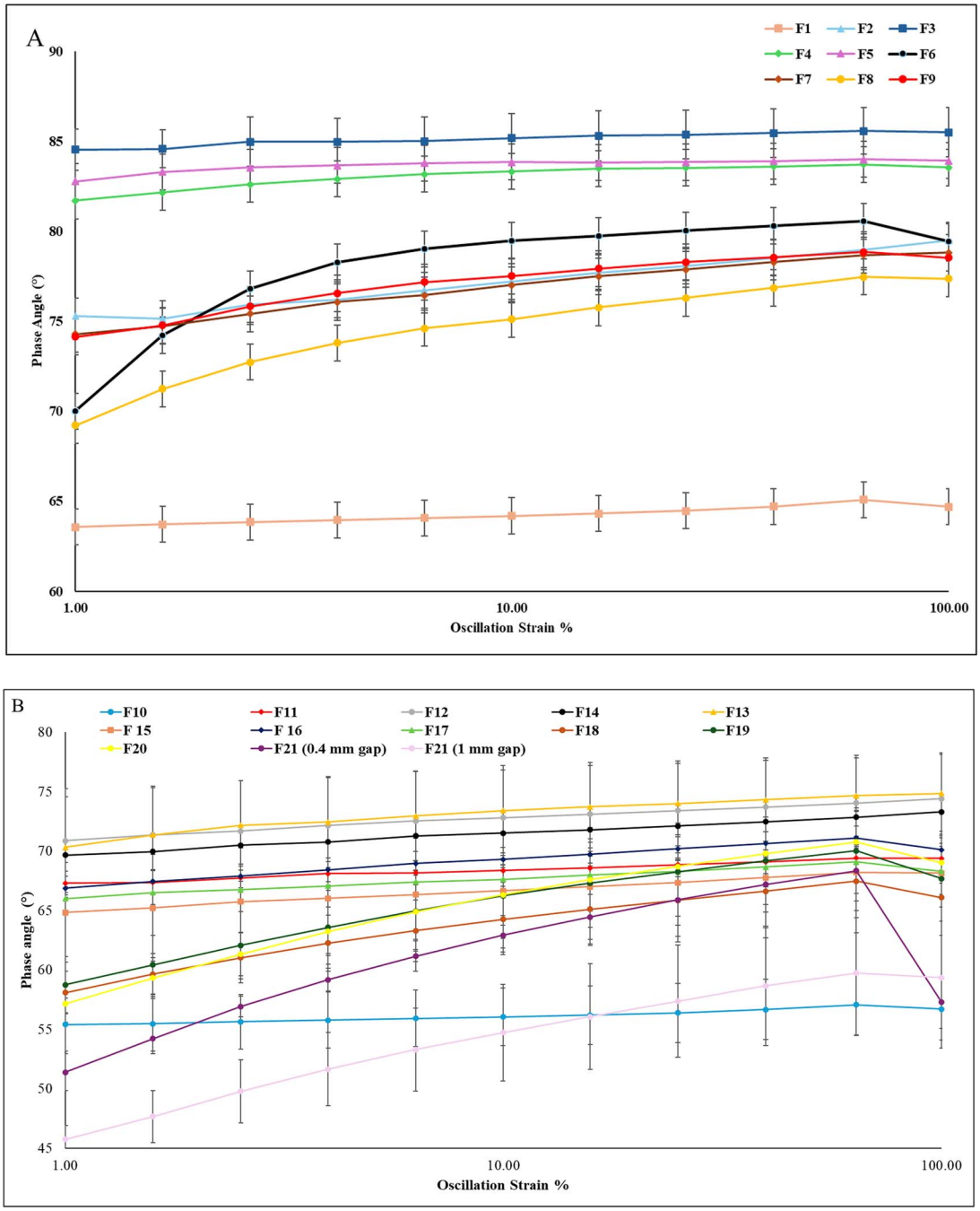

Figure 6 The phase angle versus strain of formulations: (a) F1–F9, (b) F10–F21. The phase angles of formulation F21 are given with 0.4 mm and 1 mm Peltier gaps. Data are presented as mean ± SD (n = 3).

behaviour, filler dispersion, and material-nozzle interactions. A consistent separation between the storage and loss moduli was found to be crucial for successful film printing, although favourable rheological profiles alone were not always sufficient to ensure printability. The addition of micro-composites, particularly Ch-MR at high concentrations, led to large variations in measurements, indicating the creation of heterogenous rheological regions that coincided with visible surface irregularities on filaments. These observations were consistent with the hypothesis that nozzle blockage by micro-composite aggregates represented an important failure mechanism. This interpretation was supported by SEM images of Ch-MRs and cellulose microfibres (exhibiting wide diameters) as well as increasing printing nozzle diameter from 0.4 mm to 1 mm, which resolved printing failures with high concentrations of micro-composites. Large width of Ch-MRs (~50 μm) likely contributed to nozzle obstruction at high Ch-MR concentrations, despite favourable viscoelastic properties. However, direct confirmation of this blockage mechanism would require techniques such as nozzle imaging by X-ray computed tomography. Cellulose microfibres demonstrated desirable viscoelastic properties at higher concentrations and led to more successful printing than Ch-MRs.

Overall, successful FDM printing requires not only desirable rheological properties but also a homogeneous filament structure

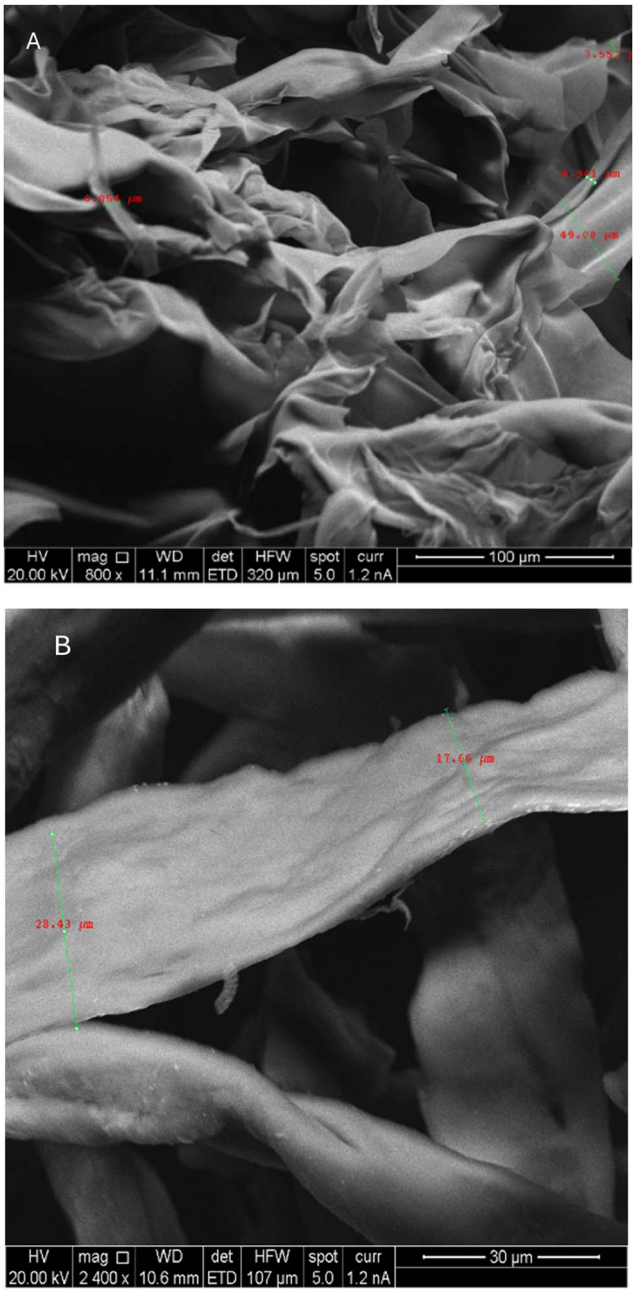

Figure 7 SEM images of Ch-MRs (a) and C500 cellulose microfibres (b) demonstrating Ch-MRs with widths in the range of 7–50 μm and C500 cellulose microfibres in the range of 20–30 μm.

and suitable printer settings, such as appropriate nozzle diameter selection, to minimize obstruction and ensure smooth extrusion.

Acknowledgements

This work is sponsored by the Libyan government, Cultural Affairs Department. We would like to express our gratitude to Weidmann Electrical Technology AG, Switzerland for supplying samples of Celova Cellulose Powders.

Author contributions

MA conducted experiments. TE designed experiments and contributed to writing and editing the manuscript. SDS, MR, and LB reviewed and edited the manuscript.

Supplementary material

Supplementary data is available at *Journal of Pharmacy and Pharmacology* online.

Conflicts of interest

None declared.

Funding

None declared.

Data availability

Data will be made available on request.

Ethics statement

This study did not involve humans or animals.

References

1. Pinho LA, Lima AL, Sa-Barreto LL. *et al.* Preformulation studies to guide the production of medicines by fused deposition modeling 3D printing. *AAPS PharmSciTech* 2021;22:263. https://doi.org/10.1208/s12249-021-02114-7
2. Alhnan MA, Okwuosa TC, Sadia M. *et al.* Emergence of 3D printed dosage forms: opportunities and challenges. *Pharm Res* 2016;33:1817–32. https://doi.org/10.1007/s11095-016-1933-1
3. Acierno D, Patti A. Fused deposition modelling (FDM) of thermoplastic-based filaments: process and rheological properties—an overview. *Materials* 2023;16:7664. https://doi.org/10.3390/ma16247664
4. Shaqour B, Samaro A, Verleije B. *et al.* Production of drug delivery systems using fused filament fabrication: a systematic review. *Pharmaceutics* 2020;12:517. https://doi.org/10.3390/pharmaceutics12060517
5. Esposito, Corcione C, Gervaso F, Scalera F. *et al.* The feasibility of printing polylactic acid–nanohydroxyapatite composites using a low-cost fused deposition modeling 3D printer. *J Appl Polym Sci* 2017;134:44656. https://doi.org/10.1002/app.44656
6. Than YM, Suriyarak S, Titapiwatanakun V. Rheological investigation of hydroxypropyl cellulose–based filaments for material extrusion 3D printing. *Polymers* 2022;14:1108. https://doi.org/10.3390/polym14061108
7. Sandanamsamy L, Harun WSW, Ishak I. *et al.* A comprehensive review on fused deposition modelling of polylactic acid. *Prog Addit Manuf* 2022;8:775–99. https://doi.org/10.1007/s40964-022-00356-w
8. Ren H, Laughton CA, Roberts CJ. *et al.* Development of an efficient approach to boost fused deposition modeling (FDM) printing of felodipine-HPMC tablets for enhanced physical stability. *Int J Pharm X* 2025;10:100394.
9. Serdeczny MP, Comminal R, Pedersen DB. *et al.* Experimental and analytical study of the polymer melt flow through the hot-end in material extrusion additive manufacturing. *Additive Manuf* 2020;32:100997. https://doi.org/10.1016/j.addma.2019.100997

10. Kotsilkova R, Tabakova S, Ivanova R. Effect of graphene nanoplatelets and multiwalled carbon nanotubes on the viscous and viscoelastic properties and printability of polylactide nanocomposites. *Mech Time-Dependent Mater* 2022;26:611–32. https://doi.org/10.1007/s11043-021-09503-2
11. Knauert ST, Douglas JF, Starr FW. The effect of nanoparticle shape on polymer-nanocomposite rheology and tensile strength. *J Polym Sci B Polym Phys* 2007;45:1882–97. https://doi.org/10.1002/polb.21176
12. Algellay M, Roberts M, Bosworth L. *et al.* The use of microribbons and micro-fibres in the formulation of 3D printed fast dissolving oral films. *Pharmaceuticals* 2023;16:79. https://doi.org/10.3390/ph16010079
13. Ehtezazi T, Algellay M, Islam Y. *et al.* The application of 3D printing in the formulation of multilayered fast dissolving oral films. *J Pharm Sci* 2018;107:1076–85. https://doi.org/10.1016/j.xphs.2017.11.019
14. Lima AL, Pires FQ, Hilgert LA. *et al.* Oscillatory shear rheology as an in-process control tool for 3D printing medicines production by fused deposition modeling. *J Manuf Process* 2022;76:850–62. https://doi.org/10.1016/j.jmapro.2022.03.001
15. Arrigo R, Frache A. FDM printability of PLA based-materials: the key role of the rheological behavior. *Polymers* 2022;14:1754. https://doi.org/10.3390/polym14091754
16. Yuan T, Zeng J, Wang B. *et al.* Cellulosic fiber: mechanical fibrillation-morphology-rheology relationships. *Cellulose* 2021; 28:7651–62. https://doi.org/10.1007/s10570-021-04034-y
17. Zotti A, Paduano T, Napolitano F. *et al.* Fused deposition modeling of polymer composites: development, properties and applications. *Polymers* 2025;17:1054. https://doi.org/10.3390/polym17081054
18. Ilieva S, Georgieva D, Petkova V. *et al.* Study and characterization of polyvinyl alcohol-based formulations for 3D printlets obtained via fused deposition modeling. *Pharmaceutics* 2023;15:1867. https://doi.org/10.3390/pharmaceutics15071867
19. Rigotti D, Fambri L, Pegoretti A. Polyvinyl alcohol reinforced with carbon nanotubes for fused deposition modeling. *J Reinf Plast Compos* 2018;37:716–27. https://doi.org/10.1177/0731684418761224
20. Zhang H, Zhang L, Zhang H. *et al.* Fibre bridging and nozzle clogging in 3D printing of discontinuous carbon fibre-reinforced polymer composites: coupled CFD-DEM modelling. *Int J Adv Manuf Technol* 2021;117:3549–62. https://doi.org/10.1007/s00170-021-07913-7
21. Kuznetsov VE, Solonin AN, Urzhumtsev OD. *et al.* Strength of PLA components fabricated with fused deposition technology using a desktop 3D printer as a function of geometrical parameters of the process. *Polymers* 2018;10:313. https://doi.org/10.3390/polym10030313
22. Ning F, Cong W, Qiu J. *et al.* Additive manufacturing of carbon fiber reinforced thermoplastic composites using fused deposition modeling. *Compos Part B* 2015;80:369–78. https://doi.org/10.1016/j.compositesb.2015.06.013
23. Yang W, Yu G. Rheological response of natural soft coastal mud under oscillatory shear loadings. *J Waterw Port Coast Ocean Eng* 2018;144:05018005. https://doi.org/10.1061/(ASCE)WW.1943-5460.0000461
24. Kattinger J, Kornely M, Ehrler J. *et al.* Analysis of melting and flow in the hot-end of a material extrusion 3D printer using X-ray computed tomography. *Additive Manuf* 2023;76:103762. https://doi.org/10.1016/j.addma.2023.103762

Journal of Pharmacy and Pharmacology, 2026, 78, rgag044
https://doi.org/10.1093/jpp/rgag044
Research Paper